RadioCycle: Deep Dual Learning based Radio Map Estimation

Yi Zheng, Tianqian Zhang, Cunyi Liao, Ji Wang, and Shouyin Liu*
Department of Electronics and Information Engineering, Central China Normal University
Wuhan, 430079 China
[e-mail: zheng saber@mails.ccnu.edu.cn, jiwang@ccnu.edu.cn, syliu@ccnu.edu.cn]
*Corresponding author: Shouyin Liu

Received September 6, 2022; revised October 21, 2022; accepted November 4, 2022; published November 30, 2022

Abstract

The estimation of radio map (RM) is a fundamental and critical task for the network planning and optimization performance of mobile communication. In this paper, a RM estimation method is proposed based on a deep dual learning structure. This method can simultaneously and accurately reconstruct the urban building map (UBM) and estimate the RM of the whole cell by only part of the measured reference signal receiving power (RSRP). Our proposed method implements UBM reconstruction task and RM estimation task by constructing a dual U-Net-based structure, which is named RadioCycle. RadioCycle jointly trains two symmetric generators of the dual structure. Further, to solve the problem of interference negative transfer in generators trained jointly for two different tasks, RadioCycle introduces a dynamic weighted averaging method to dynamically balance the learning rate of these two generators in the joint training. Eventually, the experiments demonstrate that on the UBM reconstruction task, RadioCycle achieves an F1 score of 0.950, and on the RM estimation task, RadioCycle achieves a root mean square error of 0.069. Therefore, RadioCycle can estimate both the RM and the UBM in a cell with measured RSRP for only 20% of the whole cell.

Keywords: radio map, RSRP, U-Net, urban building map, deep learning

This work was supported in part by the Key Research and Development Program of Hubei Province under Grant 2021BAA170, in part by the National Natural Science Foundation of China under Grant 62101205, in part by the Natural Science Foundation of Hubei Province under Grant 2021CFB248, and in part by the Fundamental Research Funds for the Central Universities of China under grant CCNU20QN004.

http://doi.org/10.3837/tiis.2022.11.017 **ISSN : 1976-7277**

1. Introduction

In wireless communications, Reference Signal Receiving Power (RSRP) is the average power of the received signal at the receiving point within the coverage area of the base station of a communication cell. It plays significant role in link budget, wireless communication system design, and wireless network planning and deployment. At the same time, accurate and fast RSRP estimation also provides important support for downstream tasks such as power coverage hole warning and high-precision fingerprint positioning based on RSRP. RSRP decays logarithmic-ally as the distance between the receiving point and the base station increases. In practice, radio waves are affected by the reflection, refraction, and diffraction complexes of the environment during propagation. Therefore, fast and accurate estimation of RSRP is an important challenge.

To estimate the RSRPs in a cell, RSRP data within the coverage area of a base station are usually collected using in-vehicle signal reception equipment measurements in a cell. Currently, two types of interpolation-based RSRP estimation has been widely applied. First, empirical formula-based interpolation methods, such as Cost-231 Hata [1] and standard propagation model (SPM) [2], which are based on statistical theory established by a large amount of measured data to obtain the radio propagation flux in a cell with specific environment. Due to the low computational complexity of this method, it is widely used in the estimation of RSRP for practical outdoor large-area cells. However, these methods has low estimation accuracy when the cell contains complex reflectors such as buildings, trees, etc. Second, correlation-based interpolation methods, such as K-nearest neighbor (KNN) [3], Kriging [4], tensor completion [5], make full use of the spatial correlation between the measured data and its acquisition location for RSRP estimation of the unmeasured area, and thus estimate the RSRPs of the area of interest. Since these correlation-based interpolation methods consider little radio propagation law, it does not require the physical parameters of the base station with complex and precise environmental information. Therefore, these methods are used for fast estimation of RSRP in flat open environments.

As cities have more and more high-density building clusters, the RSRP in urban scenes is more and more severely affected by the shadowing effect of buildings. The above interpolation-based RSRP estimation method does not fully consider the detailed information of the radio propagation environment and cannot accurately portray the effect of building shading on RSRP in the city, thus reducing the accuracy of the estimated RSRPs substantially.

In response to the influence of radio propagation in cities by multiple building occlusions, many researches have directly estimated the RSRP of the whole cell, i.e., the radio map (RM), from the environmental building information of the cell. Convolutional neural networks (CNNs) have been reported for this RM estimation task. [6] Considering the global information of the radio propagation environment, the whole cell environment is transformed into an environmental image containing environmental information such as building distribution and base station locations, and CNNs extract the environmental features in the environmental image through a hierarchical structure to accurately estimate the RM. At present, Ref. [7] propose a CNNs-based model RadioUNet, which generates the RM directly from the building and base station maps of the cell. Currently, RadioUNet achieves state-of-the-art performance on the public simulation dataset RadioMapSeer [7].

However, current RM estimation models in urban environment require additional building information. The measurement and collection of building data in the city add additional

workload. In fact, the measured RSRP data already contains the building distribution information. The measured RSRPs at different locations are subject to different degrees of free-space fading and shadowing effects, which can be inferred from the locations and shapes of the nearby buildings. This task of deriving building distributions from RMs is called urban building map (UBM) reconstruction. Several methods [8-10] have been used to collect RSRPs of certain cells on a large scale and for a long period of time, and then, the RMs estimated from these measured RSRPs are used to reconstruct the UBM in the city. However, a large amount of measured RSRP data using these methods is required to achieve the UBM reconstruction of a cell. In practical, large and long term RSRP collection efforts can bring huge overhead. Up to now, research progress has been made in both RM estimation and UBM reconstruction tasks. However, no researcher has yet studied how to simultaneously estimate RMs and UBMs.

Inspired by CNNs-based RM estimation and UBM reconstruction, a dual learning-based RM estimation model is proposed, called RadioCycle. RadioCycle contains two CNNs- based generators with symmetric structures, which are used to achieve the RM estimation task and the UBM reconstruction, respectively. The input of UBM reconstruction task is the incomplete measured RM, and the output is the UBM. Relatively, the UBM is used to learn to estimate the RM of the whole cell. Therefore, in this paper, RM estimation and UBM reconstruction are considered as a set of dual learning tasks, and the training dataset is fully utilized to co-train the two generators in RadioCycle simultaneously by dual deep learning. Further, there is a problem of unbalanced task training speed due to joint training of generators for two different tasks, which may lead to overfitting or inadequate task training. Also, since RM estimation and UBM reconstruction are regression and classification tasks, respectively, there is a loss function incompatibility between these two tasks, which will lead to negative transfer problem. Therefore, we introduce dynamic weighted averaging (DWA) [11] to dynamically adjust the learning rate of the loss function in each task, so that the two generators can be balanced in the joint training.

The performance of the proposed model is verified using the public dataset RadioMapSeer, which contains 56,000 maps of UBMs with their corresponding RMs for the cities of Ankara, Berlin, Glasgow, Ljubljana, London and Tel Aviv. Experiments show that on the UBM reconstruction task, RadioCycle achieves an F1 score of 0.950 and a Jaccard similarity coefficient of 0.9074. RadioCycle achieves a root mean square error of 0.069 and a normalized mean square error of 0.124 on the RM estimation task. Therefore, in the urban scenario, RadioCycle only uses the RSRP map containing the measured RSRP data to estimate the RM of the whole cell, and at the same time, RadioCycle can reconstruct the UBM of the whole cell.

2. Related work

2.1 RSRP Estimation Methods

Interpolation-based RSRP estimation is the most widely used method for estimating the RSRPs within the coverage area of a base station. RSRP estimation aims to estimate the RM of the whole cell by estimating the RSRPs of the unmeasured area from the already measured RSRP values in the area of interest. In practice, interpolation methods based on empirical formulas and correlation-based interpolation methods are usually adopted. [1-5]

The interpolation method based on empirical formula is to estimate the RSRPs of the region of interest by building a wireless propagation model that describes the slow change of

the received signal power over a long distance. The wireless propagation model usually uses the measured data to build a mathematical model of the electromagnetic environment of the cell, and the RSRP within the coverage area of the cell base station can be determined by the path loss calculated by the wireless propagation model. The interpolation method based on the formula is a wireless propagation model constructed based on measured values through mathematical statistics, which can calculate the distribution of RSRP in this environment without detailed information about the scattering environment. Essentially, this empirical model is to obtain the electromagnetic wave propagation generalization for a specific geographical environment. Since empirical models are simple to model and have good generalization in similar scenarios, they are widely used in wireless communication systems for large outdoor environments. COST-231 Hata model [1] and SPM model [2] are the most commonly used wireless propagation models for cell coverage estimation and RSRP estimation worldwide. In recent years, since many physical features affecting wireless transmission are difficult to be represented explicitly by empirical formulas, machine learning techniques have been introduced in several researches for RSRP estimation. Benefiting from the nonlinear fitting capability of machine learning, more physical features are used to estimate RSRP implicitly, resulting in more accurate RSRP estimation.

Correlation-based interpolation is an interpolation method that estimates the unmeasured RSRPs using correlations among a few measured RSRPs at different locations of a cell. This method generally treats the incomplete measured RSRPs as a highly sparse matrix. Then, the unmeasured regions are interpolated using methods such as bilinear interpolation, KNNs [3], Kriging [4] or matrix completion algorithms [5]. Considering that the task of RSRP estimation based on interpolation method can be easily associated with image processing technologies, in recent years, deep learning-based image restoration and image super-resolution algorithms have also been applied to the RSRP estimation task. Ref. [15] developed a RSRP estimation framework called Supreme based on crowdsourced data in an image super-resolution manner. Model Supreme explores the spatio-temporal relationships in historical coarse-grained measured RSRPs and estimate real-time fine-grained unmeasured RSRPs through a spatio-temporal reconstruction network. Experimental results show that Supreme shows its precision advantages on real-world datasets. However, these methods require large-scale, long-term measurement and collection of RSRPs in a cell, which can consume significant resource overhead. Also, these methods usually do not take into account the effects of obstructions in the environment such as radio blockage, reflections, and etc. Therefore, these methods generally fail to generalize to new environments of cells.

2.2 Deep Learning based Radio Map Estimation Methods

Interconversion between images of different domains has made progress in the field of computer vision. Pix2Pix is an image translation model based on conditional GANs. Pix2Pix [16] converts an image representation of an object to another representation of that object enables image mapping from domain A to domain B, thus enabling cross-domain conversion of images. For example, the color map of a purse is obtained from the contour map. StarGAN [17] declares that the image-to-image translation model should learn the mapping between different visual domains. Experiments on CelebAHQ and a new animal face dataset (AFHQ) validate the advantages of StarGAN in terms of visual quality, diversity and scalability. To address the lack of paired data during the model training step, CycleGAN [18] transforms images from one domain to another and back again. By forward cycle consistency, the inverse transformed image is identical to the original image.

Unlike the RSRP estimation task, RM estimation aims to automatically extract features affecting the RSRP of the signal reception area from the wireless propagation environment through data-driven deep learning techniques. Ref. [19] transforms the wireless propagation environment into an environmental map containing building locations, altitudes, and feature types, and propose a CNNs-based environment feature extraction model using the environment map as input. Then, the extracted environment features are fused with the physical features of the base station, and the RM of the whole cell is estimated point-by-point by a 3-layer full connection neural networks. Considering the weakness of point-by-point estimation of RM generalization, Ref. [7] proposed a cell-level CNNs-based model for RM estimation, called RadioUnet. This model directly estimates the RM of the whole cell through the UBM of the cell and the base station location. Ref. [20] considered the long-range spatial relationship of the radio propagation process and proposed a Transformer-based model for RM estimation, called RadioTrans. RadioTrans improves the estimation accuracy of RMs by better representing the relative positions of the base station, receiver, and environment through the network anchoring technique.

2.3 Urban Building Map Reconstruction Methods

The urban map reconstruction problem has important applications in non-communication areas (facilities and utility management, urban planning, navigation, etc.) as well as in communication-related areas (e.g., radio engineering, base station deployment planning, channel quality, coverage estimation, etc.). Urban map reconstruction tasks aim to reconstruct urban maps containing the shape, distribution, and height of buildings. Commonly used methods for UBM reconstruction are radio tomography [12] [13], remote sensing [14], or multi-view photo reconstruction techniques [15] which obtain geometric measurements of buildings in the urban environment. In recent years, Ref. [9] first proposed to reconstruct urban maps using real-world RMs. They employ a low-altitude UAV to measure the RSRP of outdoor ground users in urban areas and proposed a classification method to classify the measured RSRP into line-of-sight/non-line-of-sight classified data. The UBM of the whole city is then reconstructed by a set of large inequality equations. Based on this, Ref. [10] further propose to combine the depth information measured by UAVs to estimate the UBM. Then the estimated UBMs are corrected by the line-of-sight/non-line-of-sight classification data obtained from the measured RSRP data classification. Finally, the RM estimation is performed by these classification data. In practice, however, complete RMs of a small area are usually not available. A large number and long term RSRP collection effort would result in a huge overhead.

In summary, several research progresses have been achieved in both RM estimation and UBM reconstruction tasks. Up to now, no researcher has yet studied how to simultaneously estimate RMs and UBMs.

3. RadioCycle Model

3.1 Motivation

We define the set in which the measured RSRP data within the urban cell is located as Set X. The target set in which the complete RM to be reconstructed within the cell is located as Set Y. Since the measured RSRP data is a subset of the estimated RM, there is $X \subseteq Y$. The set consisting of the base station location and the UBM is defined as set Z. As shown in **Fig. 1**, the three tasks mentioned in Section 2 correspond to the three set mapping tasks.

The RM estimation task can be considered as the process of reconstructing object set Y from subset X by interpolation: $X \rightarrow Y$ The RM estimation task can be considered as the process of constructing a CNNs-based model to map from set Z to set Y based on the radio propagation rule: $Z \rightarrow Y$. Similarly, the city map reconstruction task is considered as the process of building a mapping between set X and set Z for characterizing building shape: $X \rightarrow Z$.

Due to the complex environment of urban areas, the current $X \rightarrow Y$ methods directly interpolate to estimate the RM almost without cell-level environmental information, resulting in unsatisfactory estimation accuracy of the RM. On the other hand, the current $Z \rightarrow Y$ method additionally adds the UBM containing buildings separately to obtain the high accuracy of RM estimation. Therefore, we take the set Z containing environmental information as the constraint set and propose a $X \rightarrow Z \rightarrow Y$. The UBM generated from the measured RSRP data constrains the RM estimation process and reconstructs the high accuracy RM with only the measured RSRP data, while the UBM of the cell is obtained.

Based on the physical meaning of the space in which the sets are located, we define the space in which the target set Y and its subset X are located as the radio domain, and the space in which the set Z containing building information is located as the environment domain. From the perspective of domain transfer, RM estimation is a process of translating from. In terms of domain transfer, RM estimation is a process of translating from the environment domain to the radio domain, and conversely, UBM reconstruction is a process of inversion. Therefore, in this paper, RM estimation and UBM reconstruction are considered dual tasks. Based on the measured RSRP subset X, we build an end-to-end model, called RadioCycle in order to reconstruct the UBM and the RM of the whole cell simultaneously. Two CNNs-based generators achieve the UBM reconstruction and RM estimation respectively. The two CNNs-based generators are then trained simultaneously using supervised dual learning [21]. The two trained generators can achieve the RM estimation under the condition of the environment in tandem.

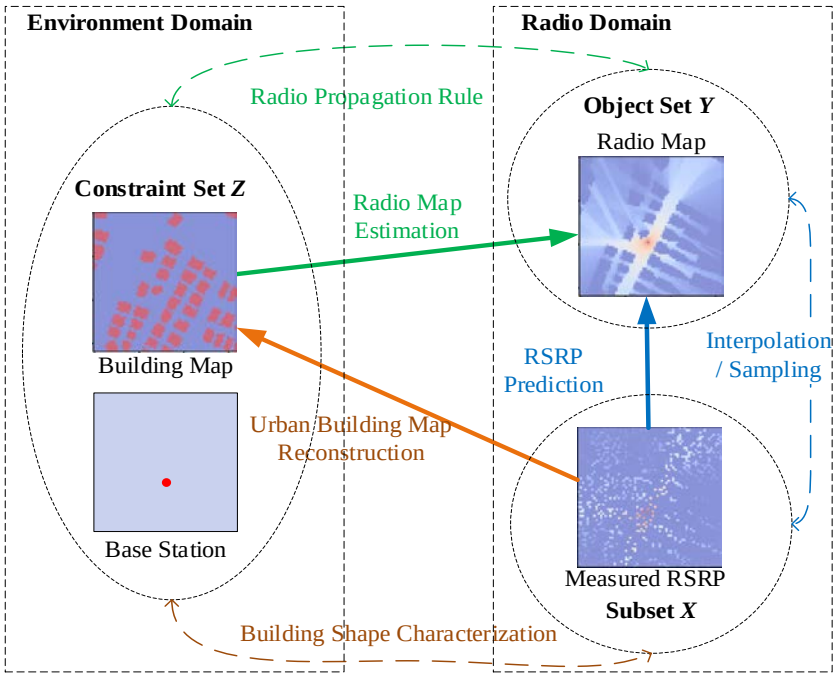

Fig. 1. Schematic diagram of domain transfer

3.2 RadioCycle Architecures

The framework of RadioCycle is shown in **Fig. 2**. The input *x* of the model represents the image, measured RSRP map, drawn according to each location of measured RSRP of a cell. There are two CNNs-based generators *G* and *F* in RadioCycle to represent the change and inversion of the environment domain to the radio domain, respectively. Generator *F* is used to learn the mapping between measured RSRP to UBM. $F(x) \rightarrow z$. Similarly, generator *G* is used to learn $G(z) \rightarrow y$. The location of the base station is considered as a point in the image. It is concatenated with the input image of the model as the input of RadioCycle.

3.2.1 Generator Structure

Depending on the output domain, the two mappings above $F(x)$ with $G(z)$ are considered as two different domain migration tasks. $G(z)$ as a RM estimation task, the output of which is a RM in which each pixel represents an RSRP value in a 1m×1m region. Since the RSRP values are continuous in the radio domain, the generator *G* is constructed as a pixel-by-pixel regression model. In the work in the Ref. [6], experiments show that the U-Net structure [22] achieves the well-performance on the RM estimation task. Therefore, the generator *G* in RadioCycle employs the same U-Net structure as that work.

$F(x)$ as a UBM reconstruction task, the output of which is the UBM of the target cell. The generator *F* in RadioCycle treats this task as a building detection task by classifying the output image pixel by pixel. Each pixel of the image represents a 1m×1m region, and generator *F* determines the presence of buildings on each pixel to further obtain the UBM of the whole cell. Therefore, the generator *F* is constructed as a pixel-by-pixel classification model. Considering that most of the regions in the input measured RSRP map of *F* are unmeasured as nulls, we use ResUNet [23] as an encoder to replace the original structure of U-Net. We hope to preserve the global information of the original map by skip connections between layers of ResUNet to alleviate the difficulty of feature extraction due to the high sparsity of the image. Therefore, the generator *F* in RadioCycle uses the ResUNet structure to complete the pixel-by-pixel classification of the measured RSRP map.

3.2.2 Running Process

The flow of RadioCycle consists of a backbone path and two auxiliary loops. As shown in **Fig. 2**, the backbone path is marked by a black directed line, and the two auxiliary loops are in green and blue respectively. First, the backbone path uses generators *F* and *G* to independently transform the radio domain and the environment domain. In the backbone path, the input *x* of generator *F* and the input *z* of generator *G* are estimated along the black line to UBM $F(x)$ and RM $G(z)$. The goal of the backbone path is to use the $F(x) \rightarrow z$ and $G(z) \rightarrow y$ mapping to complete the RM estimation and UBM reconstruction, respectively.

Second, the auxiliary loop uses a symmetric ring structure to connect generators *F* and *G*. Similar to the backbone path, generator F in the green loop converts the measured RSRP map into a UBM. $F(x)$ similar to the backbone path, generator *F* in the green loop transforms the measured RSRP map into a UBM. Then, generator *G* takes the generated $F(x)$ The goal of the green loop is to estimate the RM by $G(F(x)) \rightarrow y$ The goal of the green loop is to complete the interpolation task from the measured RSRP map to the RM. Similarly, the blue loop is the dual task of the green loop, which can be represented as $F(G(z)) \rightarrow z$. The RadioCycle connects the generators *F* and *G* through an auxiliary loop, making it an end-to-end network.

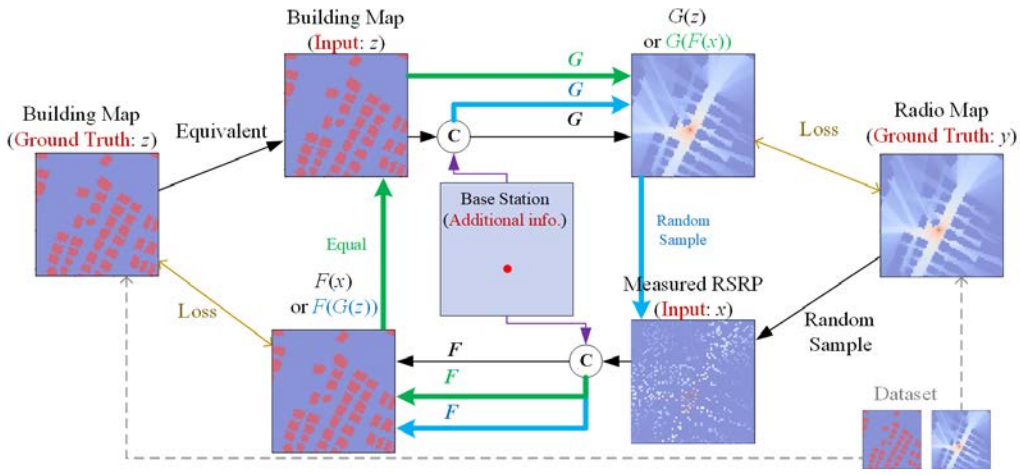

Fig. 2. RadioCycle overall structure framework

3.3 Model Training

RadioCycle as a deep supervised learning model needs to rely on a large number of pairs of data training, using gradient back-propagation algorithm to update and optimize the model parameters, and finally make the model converge to the optimal. In this section, we describe the design of the loss function and the choice of the gradient descent method used in RadioCycle training.

3.3.1 Loss Function

In RadioCycle, generator F needs to convert the Radio domain to the environment domain, while the goal of generator G is to convert the environment domain to the Radio domain. Since generators F and G perform two different domain conversion tasks, different loss functions are designed for each of the two tasks.

On the one hand, the generator G estimates the RM in a cell. Since RSRP is a continuous value, the estimation of the RM is considered as a regression fit to each pixel point in the UBM. Therefore, for the RM estimation task applying generator G, the commonly used mean squared error (MSE) loss function is used. The MSE loss can be expressed as

$$l_{MSE} = \frac{1}{N}\sum_{i=1}^{N}(p_i - g_i). \tag{1}$$

Among them, p_i and g_i correspond to the estimated and true pixel values, respectively, and N denotes the total number of pixels. During training, RadioCycle automatically adjusts the parameters of the model by a gradient descent algorithm to try to reduce the MSE between the estimated RM and the ground truth.

On the other hand, the generator F is used to estimate the distribution of buildings in the city. The reconstruction of UBM is considered a pixel-by-pixel classification of the measured RSRP map. Since the trend of the MSE Loss partial derivatives and the trend of the difference between the estimated and true values are not consistent. Therefore, for the UBM reconstruction task with the application of generator F, MSE Loss cannot be directly used as the loss function. In the binary classification problem, Binary Cross Entropy (BCE) loss is a distribution-based loss function. The gradient value calculated by BCE loss is proportional to the difference between the estimated value and the true value. BCE loss can be expressed as

$$l_{\mathrm{BCE}} = -\sum_{i=1}^{N}[g_i\, ln(p_i) + (1-g_i)\, ln(1-p_i)] \tag{2}$$

Unlike distribution-based BCE Loss, region-based Dice Loss is a loss function that calculates the similarity of an ensemble for two sample points. The dice coefficients can be expressed as

$$D = \frac{2\sum_i^N p_i g_i}{\sum_i^N {p_i}^2 + \sum_i^N {g_i}^2} \tag{3}$$

The value of each pixel in the UBM is only 0 or 1, respectively, corresponding to the presence or absence of buildings in that area. From an ensemble perspective, the dice coefficient is a measure of the overlap between two sets. The dice coefficient ranges from 0 to 1, and the larger the value, the higher the overlap between the estimated buildings and the real buildings distribution. Therefore, Dice Loss is used as a dice loss in the UBM reconstruction task to maximize the overlap between the estimated map and the real map. Dice Loss can be expressed as

$$l_{\mathrm{Dice}} = 1 - \frac{2\sum_i^N p_i g_i}{\sum_i^N {p_i}^2 + \sum_i^N {g_i}^2} \tag{4}$$

In the training of RadioCycle, dice loss and BCE loss are used as the loss function of generator *F*, called DiceBCE loss. This joint loss has three advantages: First, dice loss examines the overall overlap between the reconstructed UBM and the real one from a global perspective, while BCE is approximated pixel by pixel from a detail perspective. The overall and local complementarity of the two loss functions improves the building estimation performance of RadioCycle. Second, there is an imbalance between foreground and background samples in a sample image. Such as a cell where only a small area in a cell occupied by buildings. In this case, BCE loss cannot solve the imbalance situation of positive and negative sample. However, dice loss is not affected by the size of the foreground, and the model can still be trained. Finally, there is an imbalance in the classification content. For example, there is a large building area and a small building area in a small area. At this time, dice loss will tend to learn the large block and ignore the small sample. However, BCE loss will still learn the small samples.

Based on the above MSE Loss for regression and DiceBCE loss for classification, two loss functions are set in this paper based on each path contained in the RadioCycle structure. The inputs of the loss functions are different in different paths. For the generator *G*, loss function can be expressed as

$$l_G = l_{\mathrm{MSE}}(G(z), y) + l_{MSE}\big(G\big(F(x)\big), y\big), \tag{5}$$

where the $l_{\mathrm{MSE}}(G(z), y)$ corresponds to the black backbone path in **Fig. 2** is called estimation loss, which is used to calculate the loss of the estimated RM from the real RM. $l_{\mathrm{MSE}}\big(G\big(F(x)\big), y\big)$. Corresponding to the green pathway is called the dual loss. This dual loss function calculates the loss of the estimated RM versus the true RM based on the UBM reconstructed by the generator *F* after computing the input image.

The generator *F* is a dual process for generator *G*. Similarly, for generator *F*,

$$l_F = l_{\mathrm{DiceBCE}}(F(x), z) + l_{DiceBCE}\big(F\big(G(z)\big), z\big), \tag{6}$$

where the $l_{DiceBCE}(F(x), z)$ is used to calculate the estimated loss of the UBM. $l_{DiceBCE}\big(F\big(G(z)\big), z\big)$ is used to calculate the dual loss. In summary, the overall loss function is as follows.

$$l_{\text{total}} = \lambda_1 l_G + \lambda_2 l_F, \tag{7}$$

where the λ_1 with λ_2 are the weighting factors to adjust the loss functions of the two tasks.

3.3.2 Dynamic Weighted Average Algorithm

Since the training process of multiple tasks has the problem of difficulty to balance the task training speed, it may lead to the occurrence of the overfitting or inadequate task training, and the weights between multiple tasks are difficulty to design by hand. In addition, since RM and building estimations are regression and classification tasks, respectively, there is a loss incompatibility problem between these two tasks, which would lead to a negative transfer issue.

To address the above problems, this paper uses dynamic weighted average (DWA) [11], which is an adaptive weight adjustment method that can effectively solve the problem of difficulty in designing training weights manually. At the same time, DWA can dynamically adjust the decreasing speed of the loss function of each task by the ratio of the loss function of each task at the previous moment, and reduce the weight of the fast decreasing loss function and increase the weight of the slow decreasing loss function, so that the model can be dynamically balanced. [24]

The weights corresponding to the loss functions of the two tasks $\lambda_i(t)$ are calculated as shown below.

$$\lambda_i(t) = \frac{N \cdot exp(s_i(t-1)/T)}{\sum_n exp(s_n(t-1)/T)}, \tag{8}$$

where $r_i(s-1)$ denotes the training speed corresponding to the task i at moment t-1, and N denotes the number of tasks. When the value of T is 1, $\lambda_i(t)$ is equivalent to the probability distribution plot of the model output. Finally, the ratio of the loss function for each task is calculated, and a smaller value indicates a faster task training speed, and the model is optimized by minimizing the loss function l_{total}. The purpose of optimizing the model is achieved by minimizing the loss function.$s_i(t-1)$ The formula of the calculation is shown as follows.

$$s_n(t-1) = \frac{L_n(t-1)}{L_n(t-2)}, \tag{9}$$

where $L_n(t-1)$ denotes the loss function corresponding to task i at moment t-1.

4. Results

4.1 Datasets and Experimental Platforms

In this paper, RadioCycle is trained by the open source dataset RadioMapSeer [6], which provides 700 city maps, which are taken from OpenStreetMap in 6 different cities. Each city

map is set up with 80 base stations with omnidirectional antennas. Omnidirectional antenna base stations. The high accuracy RM corresponding to different base station locations in each city is obtained by Intelligent Ray Tracing (IRT) technique.

Data processing: RadioMapSeer provides a UBM, base station map, and RM for each simulation sample. In this paper, the RM is sampled based on uniform distribution using different sampling rates for simulating the measurement and acquisition of RSRP in a small area. Considering the real-world RSRP acquisition, the RM is sampled avoiding the interior of the building. The sampled RM is called RSRP map and is used as the input to the generator F.

Data set segmentation: According to the different cell numbers, the cells numbered 1-500 are used as the training set for training the RadioCycle model in this paper. Each cell contains 80 different base stations. The cells numbered 501-600 are used as the validation set to evaluate the convergence degree of the model during training. The cells numbered 601-700 are used as the test set to evaluate the generalization ability of the model in real scenarios.

Experimental platform: The hardware conditions of the experiment are Intel Core i7-7700K CPU and NVIDIA GeForce GTX 2080Ti 12G graphics card, the development language is Python, and the deep learning framework is PyTorch.

4.2 Evaluation Indicators

Since CycleRadio try to accomplish both the UBM reconstruction task and RM estimation task, different evaluation metrics are needed for different tasks.

Since the RM estimation task is a regression task, this paper uses Root Mean Square Error (RMSE) and Normalized Mean Square Error (MAPE) to describe the performance of RadioCycle in RM estimation task. The expressions of RMSE and NMSE are

$$\mathrm{RMSE} = \frac{1}{N}\sum_{i=1}^{N}\sqrt{\frac{\sum_{j=1}^{M}\left(\hat{r}^{(i,j)}-r^{(i,j)}\right)^2}{M}}, \tag{10}$$

$$\mathrm{NMSE} = \frac{1}{N}\sum_{i=1}^{N}\frac{\sum_{j=1}^{M}\left(\hat{r}^{(i,j)}-r^{(i,j)}\right)^2}{\sigma\left(r^{(i)}\right)}, \tag{11}$$

where, the N and M denote respectively that there are a total of N cells, and each cell has M and $r^{(i,j)}$ represents the measured RSRP value of the j-th grid in the i-th cell, and $\hat{r}^{(i,j)}$ represents the RSRP estimation result of the j-th grid in the i-th cell. $\sigma\left(r^{(i)}\right)$ represents the variance of the true RSRP value in the i-th cell.

Since the UBM reconstruction task is a dichotomous task, the Jaccard similarity coefficient and F1 Score are used to evaluate RadioCycle's UBM reconstruction ability. The Jaccard similarity coefficient, or Intersection-over-Union (IoU), reflects the overall proximity of the estimated map to the real map by measuring the degree of overlap.

$$\mathrm{Jaccard} = \frac{1}{N}\sum_{i=1}^{N}\frac{\hat{R}^i \cap R^i}{\hat{R}^i \cup R^i}, \tag{12}$$

where $\hat{R}^i$ represents the estimated map of the UBM of the i-th plot, and R^i represents the real map corresponding to it. Unlike the Jaccard similarity coefficient, the F1 score is a statistical measure of the accuracy of a binary classification model. The F1 score can be considered as a weighted average of the accuracy and recall of the model, and its range is [0,1].

Table 1. Explanatory notes for TF, TN, FN, FN

		Reconstruction results	
		Positive Example	Negative example
The ground truth	Positive Example	True Positive Example (TP)	False Negative (FN)
	Negative example	False Positive (FP)	True Negative (TN)

As shown in **Table 1**, the rows represent the estimated results and the columns represent the true situation. Depending on the different combinations of the reconstruction results and the ground truth, it is obtained that

TP: True Positive is judged to be a positive sample, and is in fact a positive sample.

FP: False Positive is judged to be a positive sample, but is in fact a negative sample.

TN: True Negative is judged to be a negative sample, and is in fact a negative sample.

FN: False Negative is judged to be a negative sample, but is in fact a positive sample.

Accuracy indicates the degree of accuracy of the estimation results, which can be expressed as the number of correctly estimated samples divided by the total number of samples.

$$\text{accuracy} = \frac{\text{TP+TN}}{\text{TP+FT+TN+FN}} \tag{13}$$

Precision is also known as accuracy. It indicates the probability of correctly estimating a positive sample among the samples that are estimated to be positive in the estimation result.

$$\text{precision} = \frac{\text{TP}}{\text{TP+FP}} \tag{14}$$

Recall, also known as check-all rate. It represents the probability of a positive sample of the original sample is correctly estimated as a positive sample in the end.

$$\text{recall} = \frac{\text{TP}}{\text{TP+FN}} \tag{15}$$

Ideally, it would be best to achieve both precision and recall, but in general, precision and recall affect each other and it is difficult to reach the optimal level at the same time. F1-score is widely used in dichotomous evaluation by considering the summation of precision and recall.

$$\text{F1 Score} = \frac{2\ \text{precision} \times \text{recall}}{\text{precision+recall}} \tag{16}$$

4.3 Performance of Urban Building Map Reconstruction

Binary classification is used to estimate whether each area in a cell is a building or not. Its estimation performance is represented in **Fig. 3**. The estimation accuracy of buildings is improved as the sampling rate increases and more RSRPs are collected in the cell. When the sampling rate exceeds 20%, the F1-score and accuracy tend to stabilize. It is worth noting that since RadioCycle incorrectly estimates most of the blank areas as buildings when the number of collected RSRPs is small, the recall rate behaves differently from the other metrics in that it decreases as the sampling rate increases.

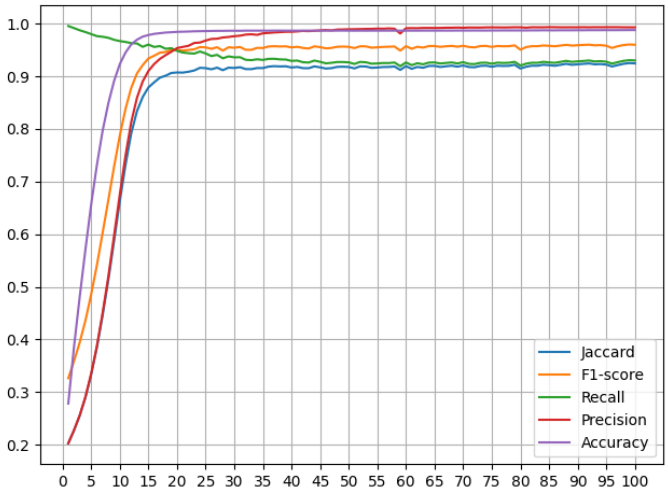

Fig. 3. UBM reconstruction performance curve of RadioCycle in test set

4.4 Performance of Radio map estimation

Considering the low estimation accuracy of the empirical and statistics-based wireless propagation model for multi-building urban scenes, to verify the RM estimation performance of RadioCycle, we compare the machine learning-based and deep learning-based RSRP estimation methods. The commonly used machine learning-based RSRP estimation methods are as follows.

The K-nearest neighbor algorithm (KNN) is a basic regression interpolation algorithm. The algorithm selects the RSRP values of the K points nearest to the estimation region from the training data. By calculating the RSRP weighted average of these K's points as the RSRP value of the interested region. The algorithm is simple in idea and insensitive to noise.

Random Forest (RF) is a cluster regression model. The algorithm builds a forest of multiple decision trees in a randomized manner, where each decision tree is unrelated to the other. When the coordinates of the new region to be estimated are input into the random forest, each decision tree is judged separately. Finally, the regression results obtained by multiple weak learners calculate the arithmetic mean to obtain the RSRP value of the region to be estimated. The algorithm is fast in training, has good generalization ability, and is not easy to fall into overfitting.

Machine learning-based regression interpolation algorithms essentially belong to RSRP estimation using the correlation of different regions in the cell. As shown in **Table 2**, since these methods mainly consider the correlation between the RSRP of a certain signal receiving point to be estimated in the cell and the surrounding points at that point, lacking environmental awareness of the whole cell, this machine learning-based point-by-point interpolation approach has poor estimation capability for the RM. At the same time, the machine learning-based regression interpolation method cannot estimate the buildings in the cell, and it needs to rely on the distribution of buildings in the area to be estimated as additional information when it is used in practice.

To further illustrate the advanced nature of the proposed RadioCycle, an interpolation network (InterpolationNet) based on the U-Net structure is considered a benchmark model for deep learning-based RM estimation methods. interpolationNet estimates the entire cell directly from the sampled real RSRP map. As shown in Table 1, the RMSE of InterpolationNet drops to the lowest value of 0.072 at a 20% sampling rate and the NMSE is 0.346. Its RMSE is close

to that of the proposed RadioCycle. Meanwhile, as shown in **Fig. 4**, InterpolationNet shows the generalization performance at different sampling rates. Both InterpolationNet and RadioCycle are trained at a 20% sampling rate. By comparing the estimation curves of InterpolationNet and RadioCycle in **Fig. 4**, it can be found that the direct deep learning-based interpolation of sampled real RSRP maps has limited generalization ability at different sampling rates. For InterpolationNet, there is a low RMSE only at 20% of the sampling rate. At other sampling rates, it causes different degrees of pattern collapse. In practical use, it is difficult to guarantee that each cell has exactly 20% of the sampling rate. Also, InterpolationNet does not give an accurate distribution of buildings in the cell as well.

Table 2. Experimental results of different methods in test set at a sampling rate of 20%

Model	Jaccard	F1-score	Recall	Precision	Accuracy	RMSE	NMSE
KNN	-	-	-	-	-	0.123	0.307
RF	-	-	-	-	-	0.114	0.239
InterpolationNet	-	-	-	-	-	0.065	0.346
RadioCycle (SL)	0.8853	0.935	0.929	0.949	0.981	0.070	0.159
RadioCycle (ML) w/o DWA	0.8826	0.934	0.930	0.944	0.981	0.072	0.143
RadioCycle (ML) w/ DWA	0.9074	0.950	0.949	0.954	0.985	0.069	0.124

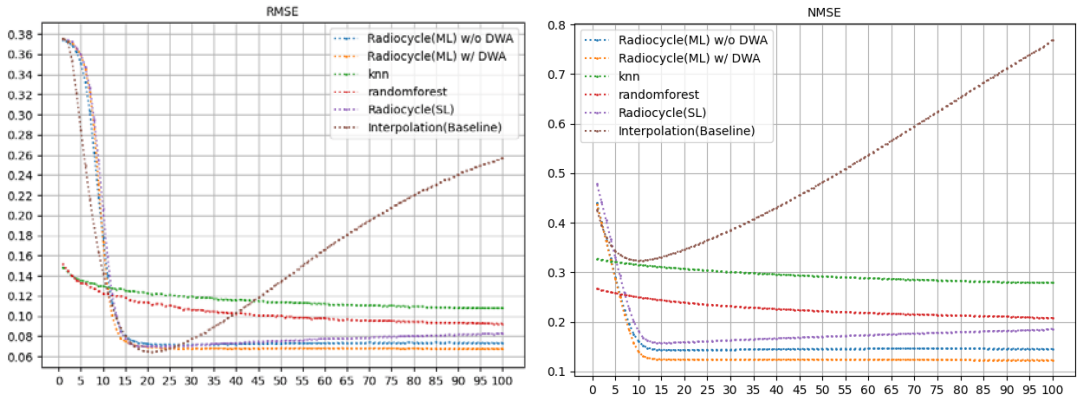

Fig. 4. RadioCycle versus different models for RM estimation performance

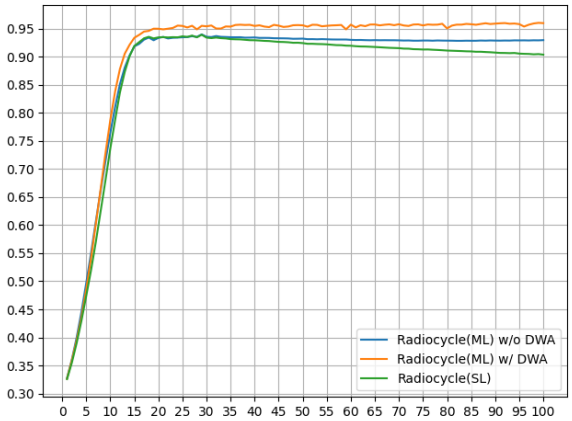

Fig. 5. Comparison of RadioCycle's performance in UBM reconstruction under different conditions of ablation experiments

In order to verify the rationality and effectiveness of the proposed RadioCycle, the ablation experiments are conducted with the dual learning loss function and the dynamic weighted average algorithm. RadioCycle (SL) represents the estimation error of the model without using the dual learning loss function, MSE loss function for generator G and DiceBCE loss function for generator F are calculated separately. RadioCycle (ML) is the RadioCycle trained with multiple loss functions by adding the dual learning loss function, where RadioCycle (ML) w/ DWA represents the RadioCycle trained with the dynamic weighted average algorithm. The results of ablation experiment are shown in **Table 2**, **Fig. 4** and **Fig. 5**, respectively. By observing **Fig. 5**, it is easy to find that the inclusion of the dual learning loss function can improve the robustness of RadioCycle in estimating buildings at different sampling rates. This is because the added dual learning loss function can make full use of the dual loss to jointly update the network parameters of generator G and generator F. And by comparing the performance curves of RadioCycle (ML) w/ DWA and RadioCycle (ML) w/o DWA, it can be found that the inclusion of dynamic weighted averaging algorithm can effectively balance the differences between classification and regression tasks. The dynamic weighted averaging algorithm dynamically adjusts the training rate so that the generators G and F. While sharing the relevant information between the two tasks, the negative transfer issue between the two tasks is mitigated, thus obtaining the best performance on both tasks simultaneously. The final estimation results are shown in **Fig. 6**.

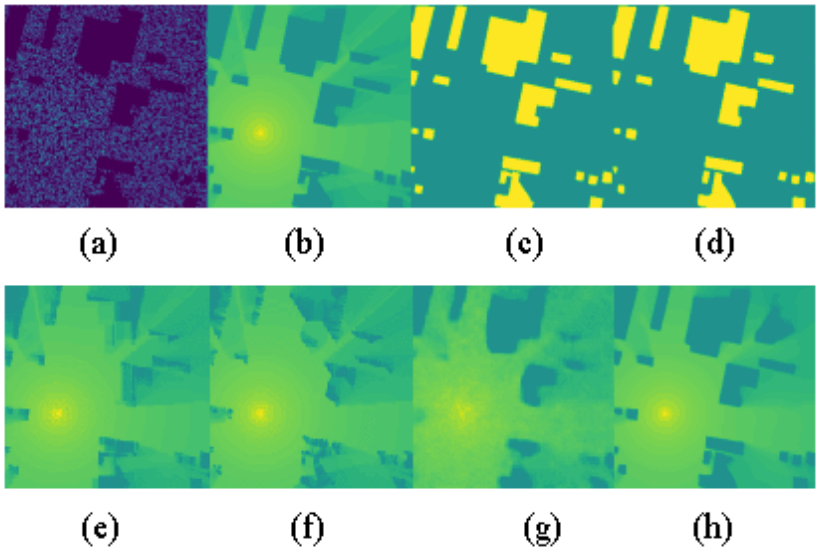

Fig. 6. Map estimation results. (a) Measured RSRP map after 20% sampling. (b) Ground truth of RMs. (c) Ground truth of UBMs. (d) UBMs estimated by RadioCycle. (e) RMs estimated by KNNs. (f) RMs estimated by RFR. (g) RMs estimated by InterpolationNet. (h) RMs estimated by RadioCycle.

5. Conclusions

In this paper, we propose a RM estimation method based on a dual learning structure. This method can simultaneously and accurately estimate the UBM and the RM of the whole cell by only part of the measured RSRP collected in the cell. This paper first considers the UBM reconstruction task and the RM estimation task as the domain transformation between the

environment domain and the radio domain problem. Then, two deep neural network-based generators are constructed to perform the UBM reconstruction task and the RM estimation task, respectively. We consider these two tasks as dual tasks. A RadioCycle model is constructed by these two generators to take advantage of the correlation between these dual tasks. Considering that the two tasks are regression task and classification task respectively, there is a negative transfer issue would interfere with joint training of RadioCycle. Thus, a dynamic weighted average is introduced to the training process of RadioCycle to mitigate this negative transfer issue and assist RadioCycle to simultaneously achieve the best performance on both dual tasks. Finally, this paper verifies on a public dataset containing 100 different cells that RadioCycle can reconstruct the UBM of a cell and estimate the RM of the whole cell in cells with only 20% of the measured RSRP.

The method proposed in this paper can still be further enhanced in future work. Since the proposed method needs to perform two different tasks simultaneously, it requires a large amount of data to train the two submodules in RadioCycle. However, due to the difficulty of obtaining real-world measurement data, the current available datasets contain a small number of cells or a large number of unmeasured areas within the cells. These measured datasets cannot support the training of RadioCycle. Research on the real measurement datasets are an important challenge for future research.

References

[1] M. Hata, “Empirical formula for propagation loss in land mobile radio services,” *IEEE Trans. Veh. Technol.*, vol. 29, no. 3, pp. 317-325, Aug. 1980. Article (CrossRef Link).

[2] H. Li, X. He, and W. He, “Review of wireless personal communications radio propagation models in high altitude mountainous areas at 2.6 GHz,” *Wireless Pers. Commun.*, vol. 101, no. 2, pp. 735-753, May 2018. Article (CrossRef Link).

[3] C. A. Oroza, Z. Zhang, T. Watteyne and S. D. Glaser, “A Machine-Learning-Based Connectivity Model for Complex Terrain Large-Scale Low-Power Wireless Deployments,” *IEEE Trans. Cogn. Commun.*, vol. 3, no. 4, pp. 576-584, Dec. 2017. Article (CrossRef Link).

[4] M. L. Stein, *Interpolation of spatial data: some theory for kriging*, USA: Springer Science & Business Media, 1999.

[5] D. Schäufele, R. L. G. Cavalcante and S. Stanczak, “Tensor Completion for Radio Map Reconstruction using Low Rank and Smoothness,” in *Proc. of 2019 IEEE 20th International Workshop on Signal Processing Advances in Wireless Communications (SPAWC)*, pp. 1-5, 2019. Article (CrossRef Link).

[6] Y. Zheng, Z. Liu, R. Huang, J. Wang, W. Xie and S. Liu, “Feature Extraction in Reference Signal Received Power Prediction Based on Convolution Neural Networks,” *IEEE Commun. Lett.*, vol. 25, no. 6, pp. 1751-1755, June 2021. Article (CrossRef Link).

[7] R. Levie, Ç. Yapar, G. Kutyniok and G. Caire, “RadioUNet: Fast Radio Map Estimation With Convolutional Neural Networks,” *IEEE Trans. Wirel. Commun.*, vol. 20, no. 6, pp. 4001-4015, June 2021. Article (CrossRef Link).

[8] H. Wu, X. Ma and S. Liu, “Designing Multi-Task Convolutional Variational Autoencoder for Radio Tomographic Imaging,” *IEEE Transactions on Circuits and Systems II: Express Briefs*, vol. 69, no. 1, pp. 219-223, Jan. 2022. Article (CrossRef Link).

[9] D. Gallup, M. Pollefeys, and J. M. Frahm, “3D Reconstruction Using an N-layer Heightmap,” in *Proc. of DAGM conference on Pattern Recognition*, pp. 1-10, 2010. Article (CrossRef Link).

[10] O. Esrafilian, R. Gangula and D. Gesbert, “Map Reconstruction in UAV Networks via Fusion of Radio and Depth Measurements,” in *Proc. of ICC 2021 - IEEE International Conference on Communications*, pp. 1-6, 2021. Article (CrossRef Link).

[11] S. Liu, E. Johns, and A. J. Davison, “End-to-End Multi-Task Learning with Attention,” in *Proc. of the IEEE/CVF conference on CVPR*, pp. 1871-1880, 2019. Article (CrossRef Link).

[12] D. Romero, D. Lee and G. B. Giannakis, "Blind Radio Tomography," *IEEE Trans. Signal Processing*, vol. 66, no. 8, pp. 2055-2069, 15 April 2018. Article (CrossRef Link).
[13] J. D. Villegas Gutierrez and C. Oestges, "Spatial Loss Field for Outdoor Micro-Cells," *IEEE Transactions on Wireless Communications*, vol. 21, no. 8, pp. 6345-6356, Aug. 2022. Article (CrossRef Link).
[14] Y. Zhang, J. Chen, S. Guo, X. Yang and G. Cui, "Building Layout Tomographic Reconstruction via Commercial WiFi Signals," *IEEE Internet of Things Journal*, vol. 8, no. 20, pp. 15500-15511, 15 Oct. 2021. Article (CrossRef Link).
[15] K. Li, J. Chen, B. Yu, Z. Shen, C. Li and S. He, "Supreme: Fine-grained Radio Map Reconstruction via Spatial-Temporal Fusion Network," in *Proc. of 2020 19th ACM/IEEE International Conference on Information Processing in Sensor Networks (IPSN)*, pp. 1-12, 2020. Article (CrossRef Link).
[16] P. Isola, J. Y. Zhu, T. Zhou, and A. A. Efros, "Image-to-Image Translation with Conditional Adversarial Networks," in *Proc. of the IEEE conference on CVPR*, pp. 1125-1134, 2018. Article (CrossRef Link).
[17] Y. Choi, M. Choi, M. Kim, J. W. Ha, S. Kim, and J. Choo, "Stargan: Unified Generative Adversarial Networks for Multi-Domain Image-to-Image Translation," in *Proc. of the IEEE conference on CVPR*, pp. 8789-8797, 2018. Article (CrossRef Link).
[18] J. Y. Zhu, T. Park, P. Isola, and A. A. Efros, "Unpaired image-to-image translation using cycle-consistent adversarial networks," in *Proc. of the IEEE international conference on computer vision*, pp. 2223-2232, 2017. Article (CrossRef Link).
[19] K. Li et al., "Model and Transfer Spatial-Temporal Knowledge for Fine-Grained Radio Map Reconstruction," *IEEE Trans. Cogn. Commun.*, vol. 8, no. 2, pp. 828-841, June 2022. Article (CrossRef Link).
[20] Y. Tian, S. Yuan, W. Chen and N. Liu, "Transformer based Radio Map Prediction Model for Dense Urban Environments," in *Proc. of 2021 13th International Symposium on Antennas, Propagation and EM Theory (ISAPE)*, pp. 1-3, 2021. Article (CrossRef Link).
[21] Z. Yi, H. Zhang, P. Tan and M. Gong, "DualGAN: Unsupervised Dual Learning for Image-to-Image Translation," in *Proc. of 2017 IEEE International Conference on Computer Vision (ICCV)*, pp. 2868-2876, 2017. Article (CrossRef Link).
[22] O. Ronneberger, P. Fischer, T. Brox, "U-net: Convolutional networks for biomedical image segmentation," in *Proc. of International Conference on Medical image computing and computer-assisted intervention*, Springer, Cham, pp. 234-241, 2015. Article (CrossRef Link).
[23] F. I. Diakogiannis, F. Waldner, P. Caccetta, and C. Wu, "ResUNet-a: A deep learning framework for semantic segmentation of remotely sensed data," *ISPRS Journal of Photogrammetry and Remote Sensing*, vol. 162, pp. 94-114, 2020. Article (CrossRef Link)
[24] Wang, H. Zhang, Q. Hu and W. Zuo, "CrabNet: Fully Task-Specific Feature Learning for One-Stage Object Detection," *IEEE Trans. Image Processing*, vol. 31, pp. 2962-2974, 2022. Article (CrossRef Link).

Yi Zheng received the B.S. degree from the School of Electronic Information and Communications, Huazhong University of Science and Technology Wuchang Branch, China, in 2015, and the M.S. degree from the College of Physical Science and Technology, Central China Normal University, China, in 2018. He is currently a doctoral student with the Department of Electronics and Information Engineering, Central China Normal University, China. His research interests include intelligent communication and deep learning.

Tianqian Zhang received the B.S. degree from the College of Physical Science and Technology, Central China Normal University, China, in 2020, and now currently studying for a Ph.D. in wireless physics at Central China Normal University, China. Her research interests include deep learning and B5G wireless communications.

Cunyi Liao received the B.S. degree from the College of Physical Science and Technology, Central China Normal University, China, in 2016, and now currently studying for a M.S. degree at Central China Normal University, China. His research interests include deep learning and autonomous driving.

Ji Wang received the B.S. degree from the School of Electronic Information and Communications, Huazhong University of Science and Technology, China, in 2008, and the Ph.D. degree from the School of Information and Communications Engineering, Beijing University of Posts and Telecommunications, China, in 2013. He is currently an Associate Professor with the Department of Electronics and Information Engineering, Central China Normal University, China. Prior to that, he held postdoctoral positions with the School of Electronic Information and Communications, Huazhong University of Science and Technology, and the Department of Electrical Engineering, Columbia University, USA. His research interests include space information networks and B5G wireless communications.

Shouyin Liu received the BS degree in physics and the MS degree in circuit and system from Central China Normal University, Wuhan, China, in 1985 and in 1988. He received the PhD degree in electronic engineering from Hanyang University, Korea, in 2005. From 1988 to 1999, he worked in the Department of Physics at Central China Normal University, Wuhan, China. Since 2005, he has been a Professor in the Department of Electronic and Information Engineering at Central China Normal University. His current research interests include wireless communication and machine learning.